



The effect of Zr content on the thermal stability, dielectric and pyroelectric behavior for lead zirconate prepared by tartrate precursor method

Osama M. Hemeda¹ · A. Tawfik¹ · A. M. Dorgham¹ · Mahmoud A. Hamad²

Received: 4 March 2019 / Accepted: 25 April 2019 / Published online: 30 April 2019
© Springer-Verlag GmbH Germany, part of Springer Nature 2019

Abstract

The series of lead titanate with various concentration of zirconium $\text{PbZr}_x\text{Ti}_{1-x}\text{O}_3$ (PZTO), where ($x=0, 0.2, 0.4$ and 0.8), have been prepared successfully by tartrate precursor method and then annealed at 1273 K in atmospheric pressure. The results showed that PZTO samples with varying composition (x) have highly phase purity and crystallized perovskite structure without pyrochlore phase in every composition. The grains of prepared samples are densely packed with few pores and the grain size increases with Zr content. The results showed also the thermal stability of $\text{PbZr}_{0.8}\text{Ti}_{0.2}\text{O}_3$ sample is higher remarkably compared to other samples with lower Zr concentration which is enhanced remarkably with Zr content. The DC resistivity and dielectric behaviors indicate that the phase transition in all the samples is diffused type. It is observed that saturation polarization and coercive field have increased with high Zr content samples ($x=0.4$ and 0.8). On the contrary, the remanent polarization has decreased slightly with high Zr content samples. Furthermore, there is a remarkable enhancement of the pyroelectric voltage for PZTO with high Zr content samples ($x=0.4$ and 0.8). Therefore, it is recommended that these prepared samples are preferable for use in pyroelectric detector applications such as infrared sensors, infrared thermometers, and laser energy sensors.

1 Introduction

In the recent times, there is a great interest in the study of ferroelectric ceramic materials due to its physical properties such as dielectric and electrocaloric, pyroelectric properties, as well as its industrial applications such as thermal sensors, thermal imaging, capacitors and computer [1–8]. Among these compounds, $\text{PbZr}_x\text{Ti}_{1-x}\text{O}_3$ (PZTO), PbTiO_3 (PTO) and PbZrO_3 ceramics have excellent physical properties such as piezoelectric, pyroelectric, and innovative characters [9–14]. Furthermore, this system is strongly dependent on the crystalline structure and its physical properties can be improved by doping [15–18]. In addition, it is used in the components of electronic devices, microelectromechanical system (MEMS) and hard disk drive [19, 20]. It is expected

that PZTO is powerful tool for engineering unprecedented optical properties that may enable future photonics innovations [1]. PZTO powders were synthesized conventionally via ceramic reaction process for oxides as starting materials [21]. But this method requires a high temperature and led to the loss of lead oxides by a large proportion, causing a reduction in the efficiency of prepared material [22]. In addition, this method has other defects such as the lack of homogeneity of ingredients, the presence of impurities during the process of grinding and large volume of the particle, which leads to reduction of the efficiency of the prepared PZTO powders. There are other ways to prepare PZTO powders such as hydrothermal, sol–gel and other chemical processes to obtain a more effective material [23–25]. However, these methods still have many disadvantages like the formation of unwanted phases during the process of calcination at high temperature, leading to the weakness of important characteristics such as dielectric and piezoelectric properties. The authors have prepared PZTO powders successfully via tartrate precursor method (TPM), showing that the piezoelectric effect and coupling factor are enhanced with low Zr content and decreases with high Zr content, recommending that the suitability of $\text{PbZr}_{0.4}\text{Ti}_{0.6}\text{O}_3$ is for developing

✉ Mahmoud A. Hamad
m_hamad76@yahoo.com

¹ Physics Department, Faculty of Science, Tanta University, Tanta, Egypt

² Basic Science Department, Higher Institute of Engineering & Technology, King Marriott Academy, Alexandria, Egypt

piezoelectric technology [26]. Therefore, these features motivate us to investigate the thermal stability, DC resistivity (ρ_{dc}), dielectric constant (ϵ') and pyroelectric properties for PZTO powders that were prepared via TPM in this work.

2 Experimental processing

2.1 Material processing

The TPM was applied for the preparation of PZTO. All chemicals used in this work, including $\text{Pb}(\text{NO}_3)_2$, TiO_2 , ZrO_2 and tartaric acid $\text{C}_4\text{H}_6\text{O}_6$ are of analytical grade with crystallite size 200 nm. The mixtures of Pb–Zr–Ti solutions were first prepared and then stirred for 15 min on hot plate magnetic stirrer, followed with addition of an aqueous solution of tartaric acid to the mixtures with continuous stirring. The solution was evaporated at 353 K with constant stirring until dryness and then inserted in a dryer oven at 373 K overnight. The dried powders were obtained as PTO precursors. Finally, the series perovskite of PZTO samples were annealed at temperature 1273 K under atmospheric pressure.

2.2 Experimental techniques

The structure properties of PZTO samples were examined by X-ray diffraction (XRD) using a Philips model (PW-1729) diffractometer where the powder specimens of the PZTO samples were exposed to Cu-K α radiation with the wavelength (λ) = 1.5406 Å. The particle size was estimated from the most intense peaks of the XRD pattern of the PZTO samples using Scherer's equation [27, 28]:

$$D = \frac{k\lambda}{\beta \cos\theta_B}, \quad (1)$$

where $k = 0.89$, β is the full width at half maximum (FWHM), and θ_B is the diffraction angle. The morphology of samples was characterized by JEOL JSM-5600 scanning electron microscope (SEM). Differential and thermogravimetric analysis (DTA and TG) characterizations were done by Perkin Elmer, Top-Loading Series STA-6000, and a 5 mg sample was heated in an alumina crucible with a heating rate of 10 K/min at N_2 atmosphere. For dielectric measurements, the two surfaces of each pellet were polished and coated with silver paste. The two-terminal method was used to measure ρ_{dc} and ϵ' for prepared samples at different temperatures using RLC bridge of type 815 B. The temperature is controlled by thermostat control heater. The dielectric hysteresis loops were measured using a modified Sawyer–Tower circuit. The samples behave as a current generator in parallel with its own resistance and capacitance. A high input impedance Keithley electrometer type shunted

by a calibrated resistor is used for measuring pyroelectric volt in the circuit. Before measuring the pyroelectric volt, the samples were poled using 2 kV potential source for 2 h. After removing the applied field, the polarized sample is ready for measurements.

3 Results and discussion

3.1 Structure properties

Figure 1 shows XRD patterns collected on annealed disks of PZTO with varying composition (x), showing highly crystallized perovskite structure, indicating the rhombohedral compositions with $x=0.0$ and 0.2, the tetragonal composition with $x=0.80$, and a two-phase mixture of tetragonal and rhombohedral phases with $x=0.4$. Furthermore, there is no pyrochlore phase in every composition, which is usually caused by off-stoichiometric precursor solution or the volatilization of PbO during the heating process. Therefore, PZTO samples prepared by tartrate method have high quality and the actual composition would be favored for ferroelectric properties. This means that the PZTO powders with high phase purity can be obtained by tartrate method. On the other hand, the relative intensities of (101) peak, which correspond to the inclined c -axis orientation is higher than other peaks. The FWHM of (101) peak shows a jump at composition with $x=0.40$ due to the combination effects of crystallite size and micro-strains.

It can be seen that peak (002) at angle $2\theta=45^\circ$ splits into two lines which is signature of tetragonal phase. The peak (200) at $2\theta=47^\circ$ becomes lower intensity by increasing Zr content which completely disappeared when tetragonal phase is completely formed. The PZTO shows a two-phase coexistence characteristic, and leads to two spontaneous strains which contribute to the PZTO at around morphotropic phase boundary (MPB). However, the volume fraction

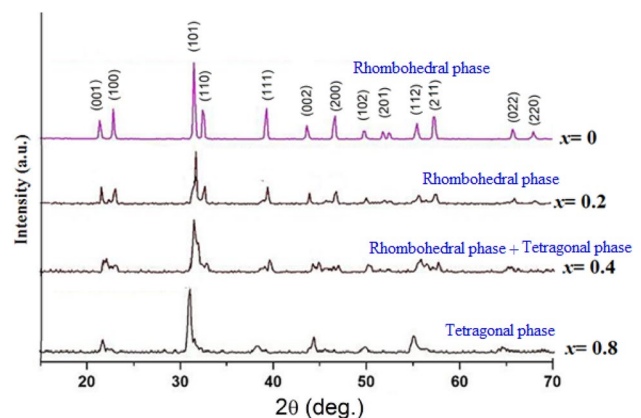


Fig. 1 The XRD patterns of PTO and PZTO samples

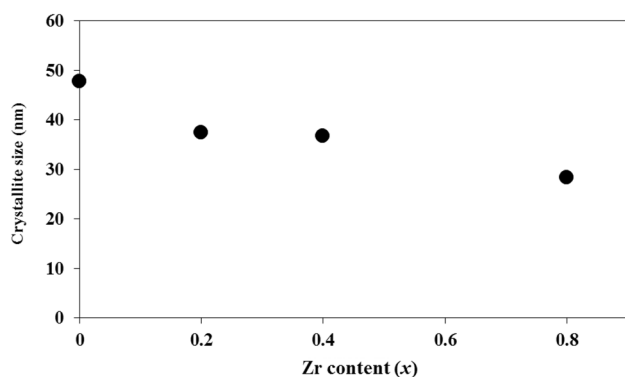


Fig. 2 The average crystallite size vs. Zr content for PZTO samples

of two phases cannot be quantified precisely due to the resolution limits of the diffractometer. The domain structure miniaturize to nano-scale could be another reason to broaden the peak width. This combination effect of crystallite size, nano-domains and micro-strains could be the reason that the FWHM at composition with $x=0.40$ is almost double the size than the rest of the compositions. These results indicate that for PZTO samples have polycrystalline structure with random grain orientation. Figure 2 shows that the average crystallite size decreases with Zr content due to increase in lattice strain because of ionic size mismatch as ionic size of the Zr^{+2} (0.89 \AA) is more than that of Ti^{+3} (0.67 \AA) [29].

3.2 Scanning electron microscope (SEM)

Figure 3 shows SEM images of the surface morphology of PZTO samples with different Zr contents ($x=0, 0.2$ and 0.8). It is clear from the nature of micrograph for each sample that the grains are densely packed with few pores and are irregular in shape and different in size. Furthermore, the grain size increases with Zr content.

3.3 Thermal analysis

Figure 4 shows that the DTA and TGA curves for the PTO and PZTO samples are performed at heating rate $10 \text{ }^\circ\text{C}/\text{min}$.

The DTA curve for the pure PTO shows an endothermic peak at about 753 K which corresponds to the structural phase transition from the tetragonal to cubic phase as shown in Fig. 4a. Figure 4b shows main stages in the decomposition reaction. The first weight loss below 473 K corresponds to the decomposition of tartrate nitrate hydroxides and the formation of PbO groups [30]. After that there was a slight weight loss due to burning of the residual organic groups and carbon decomposition. The second stage is at about 643 K , indicating the elimination of the last organic residues, such as hydroxyls, with a simultaneous onset of the formation of PZTO and the crystallization process. Thus, the (DTA,

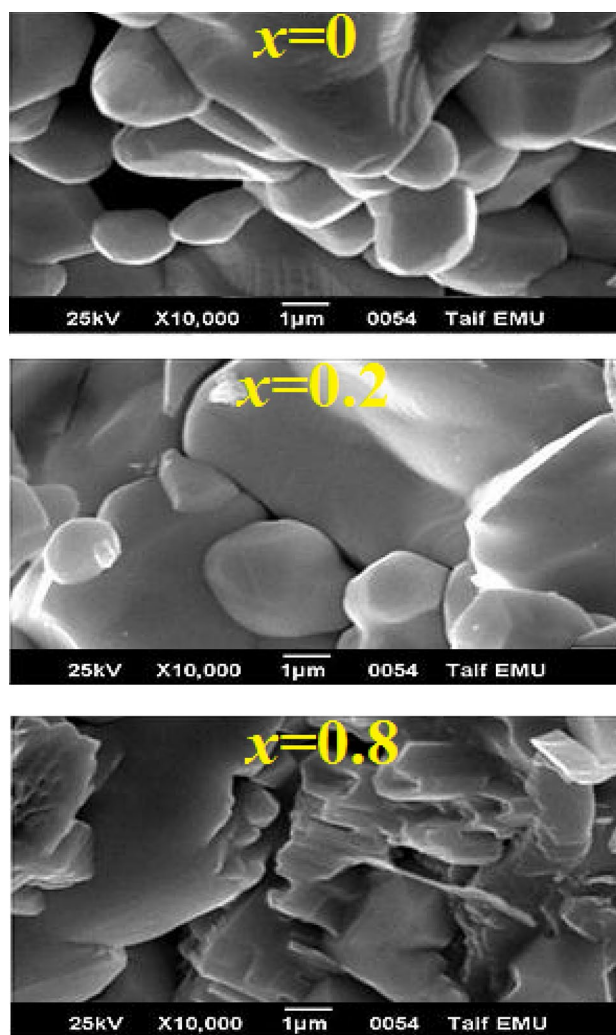


Fig. 3 SEM images of the surface morphology of PTO and PZTO samples

TGA) curves confirm the formation of PZTO perovskite structure by tartrate methods at about 673 K . The third stage around 1073 K corresponds to the decomposition of PZTO and PbO [30]. Moreover, Fig. 4b shows that the temperature of the degradation and thermal stability of $PbZr_{0.8}Ti_{0.2}O_3$ sample are higher remarkably compared to other samples with lower Zr concentration.

3.4 DC electrical resistivity (ρ_{dc})

Figure 5 shows the variations of logarithmic ρ_{dc} vs. reciprocal of temperature ($10^3/T$) for PTO and PZTO samples. The relation between resistivity and temperature can be expressed by the relation

$$\rho = \rho_0 e^{\left(\frac{E_a}{k_B T}\right)}, \quad (2)$$

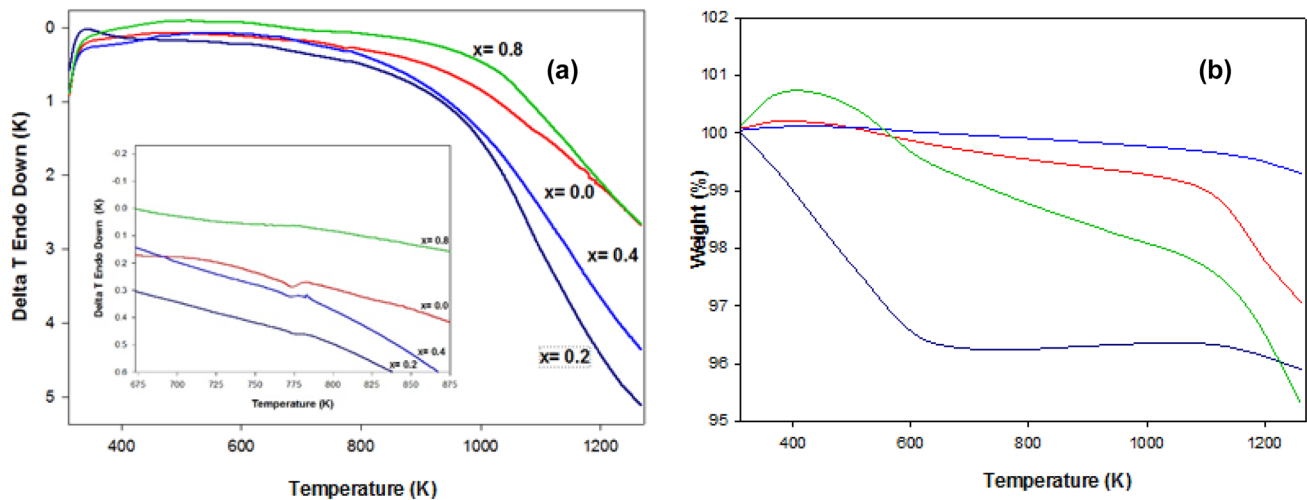


Fig. 4 Thermal analysis curves of PTO and PZTO samples **a** DTA and **b** TGA

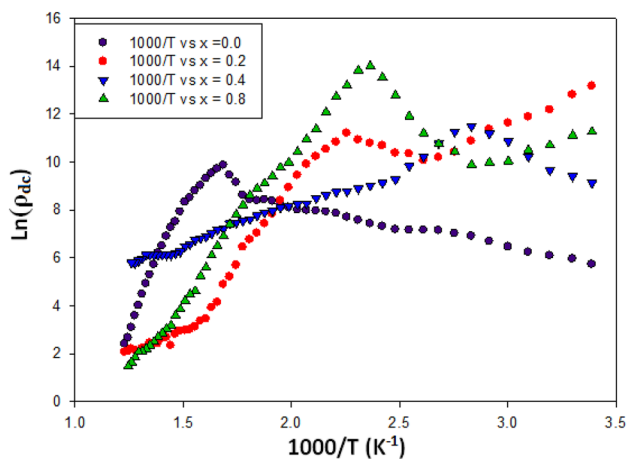


Fig. 5 $\ln(\rho_{dc})$ vs. reciprocal of temperature for PTO and PZTO samples

where ρ_0 is the pure exponent factor, E_a is the activation energy and k_B is Boltzmann constant.

From Fig. 5, it is observed that the conduction mechanism changes from low-temperature to high-temperature regions. The decrease in ρ_{dc} is observed sharply at high-temperature region due to the presence of hopping electrons which is thermally activated. The ρ_{dc} at low temperature < 600 K is due to impurities whereas at higher temperature due to polaron hopping between $Ti^{+4} \rightarrow Ti^{+3}$. Furthermore, at low temperature, the crystal structure of the samples has tetragonal phase whereas at high temperature after T_c between 700 and 770 K, the structure becomes cubic phase. The calculated E_a values are around 0.58 eV which clearly suggests that the conduction is due to polaron hopping [31].

3.5 Dielectric constant (ϵ')

Figure 6 shows the temperature dependence of ϵ' for PTO and PZTO samples. As in normal ferroelectrics, ϵ' increases gradually to a maximum value (ϵ'_{max}) with increase of temperature up to T_c due to its high resistivity, the presence of impurities and defects in the materials, and then it decreases for all samples, indicating the phase transition in PZTO between 700 and 750 K. Qualitatively, the broadened peaks indicate that the phase transition in all the cases is diffused type. Furthermore, T_c and ϵ'_{max} of the PZTO monotonically decrease with the increase of ionic concentration of Zr. This is due to the increase in the grain size with concentration of Zr, leading to low space charges and defects that impede the domain wall mobility [32, 33]. At 1 kHz frequency, ϵ' is higher than corresponding values at 10 kHz frequency. This due to the fact of that as the frequency increases, the dipole polarization effect will be lower and then the polarization is more dependent on the electronic polarization [34].

3.6 The ferroelectric hysteresis-loop

Figure 7 shows the room temperature ferroelectric hysteresis loops for PTO and PZTO samples, indicating an excellent ferroelectric behavior. Beginning from PTO, it is observed that saturation polarization (P_s) and coercive field (E_c) have increased with high Zr content samples ($x=0.4$ and 0.8). On the contrary, remanent polarization (P_r) has decreased with high Zr content samples.

The higher value of P_s and E_c for high Zr content samples as compared to undoped PTO ceramics can be attributed to Ti vacancies formed due to Zr ion substitution. These Ti vacancies are negatively charged and these get paired with Zr^{2+} ions to form defect poles. These defect

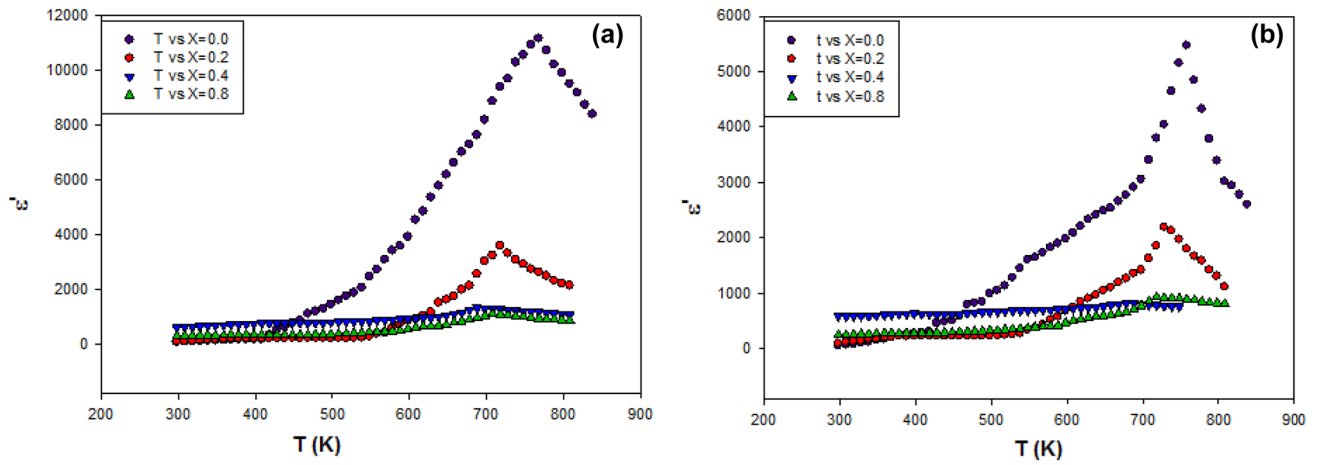


Fig. 6 ϵ'' vs. temperature for PTO and PZTO samples: a at 1 kHz, b at 10 kHz

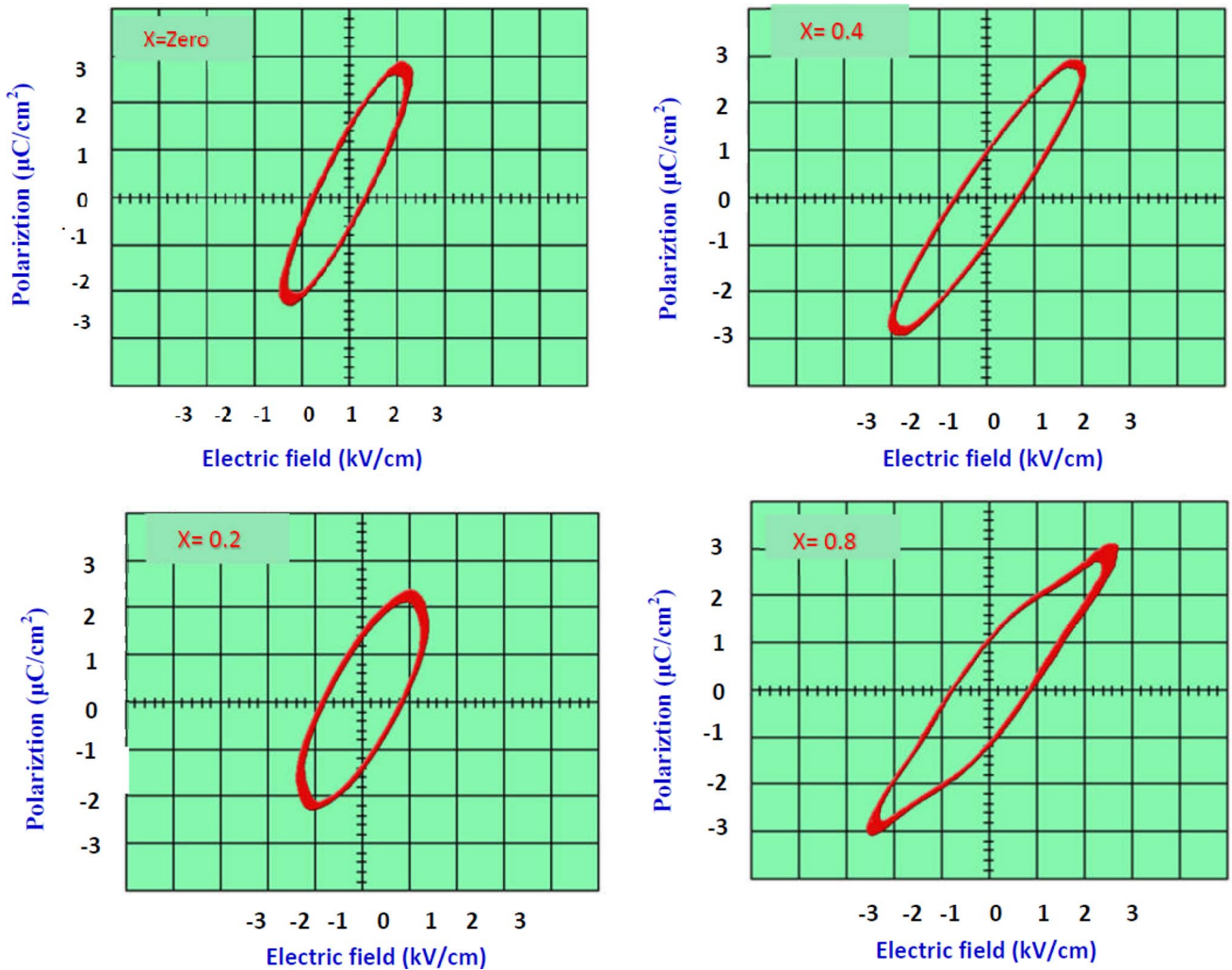


Fig. 7 Ferroelectric hysteresis-loop for PTO and PZTO samples

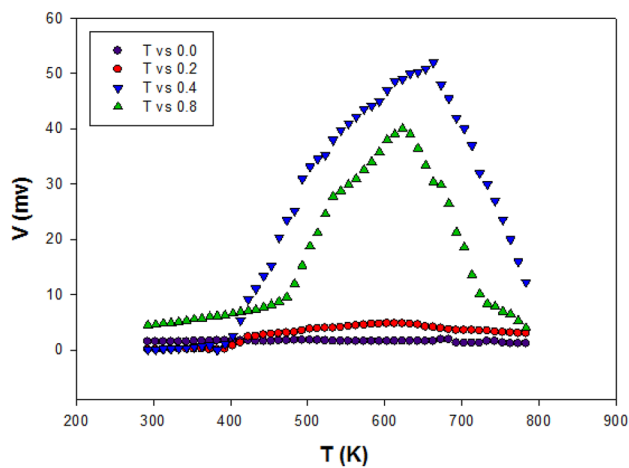


Fig. 8 Pyroelectric voltage vs. temperature for PTO and PZTO samples

poles can be aligned when there is an applied electric field. This creates a larger polarization and hence can explain why highly doped PZTO has larger P_s than PTO, as observed in our samples. The low decrease of P_r in highly doped PZTO samples can be attributed to increase in grain size as it is indicated in SEM. Moreover, there are rhombohedral compositions with $x = 0.1$ and 0.2 and the tetragonal composition with $x = 0.80$, and a two-phase mixture of tetragonal and rhombohedral phases with $x = 0.4$ as it is indicated in XRD.

3.7 Pyroelectric voltage

Figure 8 shows the pyroelectric voltage for PTO and PZTO samples. The pyroelectric voltage increases with increase of temperature up to T_c due to the displacement of ion under thermal agitation leading to the increase in ionic distance and dipole moment resulting in the increase on polarization at T_c and then it decreases for all samples due to the structural phase transition from tetragonal to cubic phase. Furthermore, there is a remarkable enhancement of the pyroelectric voltage for PZTO with high Zr content samples ($x = 0.4$ and 0.8). Therefore, it is recommended that these prepared samples are preferable for use in pyroelectric detector applications with excellent long-term stability like powerful thermal infrared detectors for detection the typical spectral emission of burning material. Furthermore, it can be used in passive infrared sensors, infrared thermometers, laser energy sensors and sensitive elements based on MEMS technology.

4 Conclusion

TPM is a simple and effective method to prepare PZTO highly phase purity and crystallized perovskite structure without pyrochlore phase in every composition. The thermal stability of $\text{PbZr}_{0.8}\text{Ti}_{0.2}\text{O}_3$ sample is higher remarkably compared to other samples with lower Zr concentration. The phase transition in all the samples is diffused type. The high Zr content improves P_s and E_c while P_r has been reduced slightly with Zr content. Furthermore, there is a remarkable enhancement of the pyroelectric voltage for PZTO with high Zr content samples, recommending that high Zr content samples are useful in pyroelectric detector applications.

References

- H. Cui, R. Hensleigh, D. Yao, D. Maurya, P. Kumar, M.G. Kang, X.R. Zheng, *Nat. Mater.* **18**, 234–241 (2019)
- M. Li, H. Tang, X. materials. *Nat. Mater.* **18**, 9 (2019)
- M.A. Hamad, *J. Adv. Dielect.* **4**, 1450026 (2014)
- M.A. Hamad, *J. Adv. Dielect.* **3**, 1350029 (2013)
- M.A. Hamad, *Appl. Phys. Lett.* **102**, 142908 (2013)
- M.A. Hamad, *Phase Trans.* **86**, 307 (2013)
- A.H. El-Sayed, M.A. Hamad, “Tailoring thermomagnetic properties in $\text{Pb}(\text{Zr}_{0.52}\text{Ti}_{0.48})\text{O}_3\text{-Ni}_{(1-x)}\text{Zn}_x\text{Fe}_2\text{O}_4$ ”, *Phase Trans.* (2019). <https://doi.org/10.1080/01411594.2019.15970969>
- M.A. Hamad, *J. Adv. Ceram.* **2**, 308 (2013)
- S. Lee, T. Kang, W. Lee, M.M. Afandi, J. Ryu, J. Kim, *Sci. Rep.* **8**, 301 (2018)
- M.A. Hamad, *J. Electron. Mater.* **43**, 522 (2014)
- E. Koushki, J. Baedi, A. Tasbandi, *J. Electron. Mater.* **48**, 1066 (2019)
- F.Z. El Fatnani, M.H. Mazroui, D. Guyomar, *Eur. Phys. J. Plus* **133**, 519 (2018)
- Q. Wang, C.R. Bowen, W. Lei, H. Zhang, B. Xie, S. Qiu, S. Jiang, *J. Mater. Chem. A* **6**, 5040–5051 (2018)
- M.A. Hamad, *Int. J. Thermophys.* **34**, 1158 (2013)
- S.W. Ko, W. Zhu, C. Fragkiadakis, T. Borman, K. Wang, P. Mardilovich, S. Trolier-McKinstry, *J. Am. Ceram. Soc.* **102**, 1211 (2019)
- X. Chen, S. Yan, H. Nie, F. Cao, G. Wang, X. Dong, *J. Alloys Compd.* **779**, 450–455 (2019)
- K. Nomura, W. Wang, H. Yamaguchi, K. Nakamura, T. Eshita, S. Ozawa, M. Kojima, *Jpn. J. Appl. Phys.* **57**, 11UF01 (2018)
- M.A. Hamad, *J. Electron. Mater.* **46**, 888 (2017)
- D.M. Potrepka, M. Rivas, H. Yu, M. Aindow, G.R. Fox, R.G. Polcawich, *J. Mater. Sci. Mater. Electron.* **29**, 11367 (2018)
- G. Zhang, Y. Yang, H. Li, S. Shen, S. Wu, *Microsyst. Technol.* **22**, 1467 (2016)
- S.S. Chandratreya, R.M. Fulrath, J.A. Pask, *J. Am. Ceram. Soc.* **64**, 422 (1981)
- S. Kim, G.S. Lee, T.R. Shrout, S. Venkataramani, *J. Mater. Sci.* **26**, 4411 (1991)
- S.B. Cho, M. Oledzka, R.E. Riman, *J. Cryst. Growth* **226**, 313–326 (2001)
- A. Khorsand Zak, W.H. Abd Majid, *Ceram. Int.* **36**, 1905 (2010)
- J. Hao, Z. Xu, R. Chu, Y. Zhang, Q. Chen, P. Fu, Q. Yin, *Mater. Des.* **31**, 3146 (2010)

26. A. Tawfik, O.M. Hemed, A.M.A. Henaish, A.M. Dorgham, *Mater. Chem. Phys.* **211**, 1 (2018)
27. P. Klug, L.E. Alexander, *Direction Procedures for Polycrystalline and Amorphous Materials* (Wiley, New York, 1954)
28. B. Choudhury, A. Choudhury, *Mater. Chem. Phys.* **131**, 666 (2012)
29. R.D. Shannon, *Acta Crystallogr.* **A32**, 751 (1976)
30. D.K. Mahato, R.K. Chaudhary, N.N. Das, S.C. Srivastava, *Indian J. Pure Appl. Phys.* **41**, 767 (2003)
31. M.I. Klinger, *J. Phys.* **C8**, 3595 (1975)
32. K. Okazaki, K. Nagata, *J. Am. Ceram. Soc.* **82**, 56 (1973)
33. R. Khazanchi, S. Sharma, T.C. Goel, *J. Electroceram.* **14**, 113 (2005)
34. M.S. Zakerhamidi, A. Ghanadzadeh, M. Moghadam, *Chem. Sci. Trans.* **1**, 1 (2012)

Publisher's Note Springer Nature remains neutral with regard to jurisdictional claims in published maps and institutional affiliations.